Supporting Information

Synergistically Boosting Oxygen Evolution Reaction of Fe-MOF by Ni Doping and Fluorination

Hui Liu[a], Meng Zha[a,b], Zong Liu[a], Jingqi Tian[a], Guangzhi Hu[b] and Ligang Feng[a*]

a. School of Chemistry and Chemical Engineering, Yangzhou University, Yangzhou 225002, PR China.

b. Institute for Ecological Research and Pollution Control of Plateau Lakes, School of Ecology and Environmental Science, Yunnan University, Kunming 650504, China.

Email: ligang.feng@yzu.edu.cn; fenglg11@gmail.com (L Feng*);

1. Experimental section

1.1 Materials

All chemicals used were of analytical grade and used as received. Nickel nitrate hexahydrate ($Ni(NO_3)_2 \cdot 6H_2O$), iron chloride hexahydrate ($FeCl_3 \cdot 6H_2O$), urea (NH_2CONH_2), fumaric acid ($C_4H_4O_4$), and ammonium fluoride (NH_4F) were bought from Aladdin Chemistry Co Ltd. Nafion (5 wt%) was from Sigma-Aldrich Co. Ultrapure water (resistivity ≥ 18.2 MΩ cm^{-1}) was used to prepare the solutions.

1.2 Catalyst preparation

1.2.1 Preparation of MIL-88A Fe MOF

$FeCl_3 \cdot 6H_2O$ (4 mmol) and fumaric acid (4 mmol) were dissolved in 20 mL ultrapure water. The mixture was then transferred into a Teflon reaction kettle, placed in an autoclave, and heated to 65 °C for 4 h. Finally, the product was washed by ultrapure water several times and dried at 60 °C for 12 h in the vacuum oven.

1.2.2 Preparation of Ni-doped Fe MOF

Ni-doped Fe MOF was synthesized according to a previously reported method with modifications.[1-3] The obtained MIL-88A (150 mg) was dispersed in 8 mL of ethanol (solution A). 300 mg of $Ni(NO_3)_2 \cdot 6H_2O$ and 200 mg of urea were dissolved in 12 mL of ultrapure water (solution B). Then, solution A and solution B were mixed via stirring at room temperature (solution C). At last, the solution C was transferred into a Teflon reaction kettle, placed in an autoclave, and heated at 90 ^oC for 5.5 h. The product was washed with ultrapure water and ethanol for 3 times by centrifugation and dried at 70 ^oC for 12 h in the vacuum oven.

1.2.3 Preparation of Ni-doped FeF_2

Ni-doped MIL-88A Fe MOF and NH_4F with a mass ratio of 1:10 were placed in one closed porcelain crucible, NH_4F was at the upstream side of the furnace. Then it was heated to 450^oC with a heating rate of 3 ^oC/min and kept for 2 h in N_2 protection. After cooling to room temperature, the black product was collected by centrifugation and washed with ultrapure water several times. The Ni doped FeF_2 was finally obtained after drying for 12 h at 60 ^oC in the vacuum oven.

1.2.4 Preparation of FeF_2

The FeF_2 was synthesized in the same way to Ni-doped FeF_2 except the Ni-doped MIL-88A was replaced by MIL-88A Fe MOF.

1.3 Physical characterization

Powder X-ray diffraction (XRD) patterns were tested on a Bruker D8 Advance powder X-ray diffractometer using a Cu Kα (λ = 1.5405 Å) radiation source operating at 40 kV and 40 mA, and at a scanning rate of 5 ° min^{-1}. The morphology and microstructure of catalysts were analyzed by scanning electron microscopy (FESEM, Hitachi, S-4800 II, Japan). All transmission electron microscopy (TEM) and high-resolution TEM (HRTEM) measurements of Ni-doped FeF_2 were conducted on a TECNAI G2 operating at 300 kV. The energy dispersive X-ray detector spectrum (EDX) images were obtained on a TECNAI G2 transmission electron microscope equipped with an EDXA detector. All X-Ray photoelectron spectroscopy (XPS) measurements were carried out on a Kratos XSAM-800 spectrometer with an Al Kα radiation source. Fourier transform infrared (FT-IR) spectra were recorded on a Tensor27 using KBr disks.

1.4 Electrochemical measurements

All the electrochemical measurements were tested in a typical three-electrode system linked to a Bio-Logic SAS analyser (France). Our catalysts electrode served as the working electrode with a graphite rod as the counter electrode; a saturated calomel electrode (SCE) as the reference electrode was employed through a double salt-bridge and luggin capillary and it was calibrated before and after the experiments to ensure the accuracy. A glassy carbon electrode (3.0 mm diameter) was used to support the catalysts. The working electrode was prepared as follows. 5 mg of the specific catalyst (IrO_2, Fe MOF, Ni-doped Fe MOF, FeF_2 and Ni-doped FeF_2) were dispersed entirely into the mixture of 950 μL ethanol and 50 μL Nafion (5 wt%). After sonicated for 30 min to make a homogeneous solution, 10 μL ink was dropped into the surface of the glassy carbon electrode. The electrolyte (1M KOH) was saturated by N_2 atmosphere before use.

All the potentials used were converted into RHE. (E(RHE) = E(SCE) +0.0591*pH+0.24V)

The catalytic performance of the samples for OER was evaluated by linear scan voltammetry (LSV), the scanning rate was 5 mV s^{-1}. Electrochemical impedance spectroscopy (EIS) which was recorded in the above three-electrode cell with the frequency varies from 1000 kHz to 10 mHz with an amplitude of 5 mV.

To estimate the effective surface areas of catalysts, we measured the double-layer capacitance (C_{dl}) by cyclic voltammetry (CV) method through varying the scan rate (20, 40, 60, 80 and 100 mV s^{-1}) in the non-Faradaic region from 0.83 to 1.03 V vs RHE. By plotting $\Delta j = 1/2(j_{anodic} - j_{cathodic})$ at the middle potential (0.93 V) against the scanning rates, the linear slope is the double layer. j_{anodic} and $j_{cathodic}$ are anodic and cathodic current density at anode (>0) and cathode (<0), respectively. The electrochemical active surface area (ECSA) was calculated by normalizing the C_{dl} (in mF) to the specific capacitance of 40 μF cm^{-2}. The roughness Factor (RF) is obtained from the ratio of ECSA to the geometric surface area (0.07cm^2) of the electrode.[4] The stability was tested for 1000 cycles from 1.03 to 1.63 V at the constant scan rate of 150 mV s^{-1}. After 1000 cycles, the stable polarization curve was recorded for comparison with the initial curve. To estimate the stability of the catalysts, the chronoamperometry (CA) was performed at a potential of 1.51 V vs. RHE for 25 h. All tests were measured at room temperature (about 25 ^oC). All LSV curves were corrected with 85% iR compensation.

1.5 Turnover frequency (TOF) calculation

The TOF values were calculated from the following equation:

$$TOF=(j \times A)/(4 \times F \times n)$$

j is the current density. A is the surface area of the electrode. F is the Faraday constant (96485 C mol^{-1}), the number 4 means 4 mole electrons per mole O_2, n is the number of moles of active materials deposited onto the electrode.[5]

1.6 Faradaic efficiency calculation

A gas-tight electrochemical cell coupling with a gas burette was carried out to verify the faradaic yield of Ni doped FeF_2. A constant potential at 1.51V was applied on the electrode and the volume of the evolved gas was recorded synchronously. Thus, the faradaic yield was calculated from the

ratio of the recorded gas volume to the theoretical gas volume during the charge passed through the electrode.

$$Faradaic\ yield = \frac{V_{experimental}}{V_{theoretical}} = \frac{V_{experimental}}{\frac{1}{4} \times \frac{Q}{F} \times V_m}$$

where Q is the charge passed through the electrode, F is Faraday constant (96485 C mol^{-1}), the number 4 means 4 mole electrons per mole O_2, V_m is molar volume of gas (24.5 L mol^{-1}, 298 K, 101 KPa).

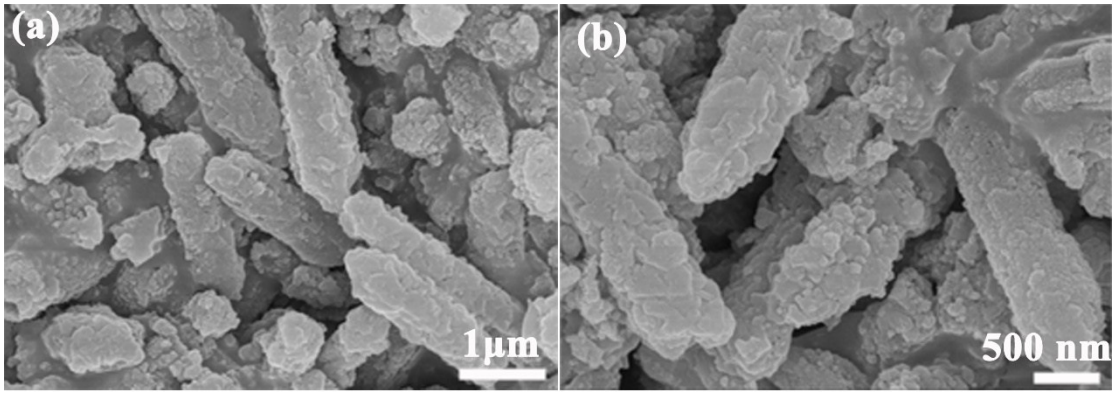

Figure S1. SEM images of Ni doped FeF_2 (a-b).

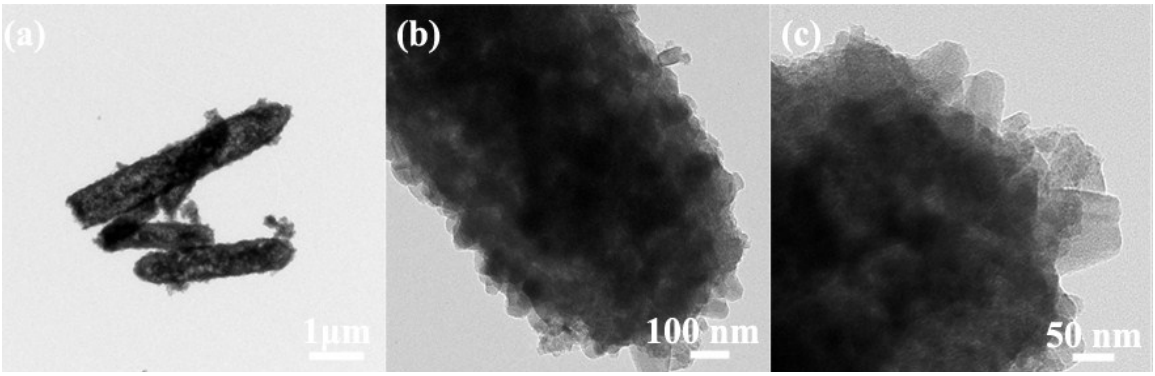

Figure S2. TEM images of Ni-doped FeF_2 (a-c).

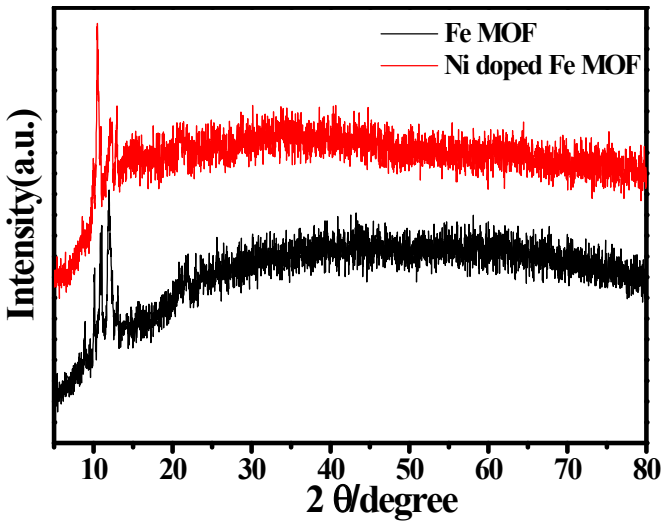

Figure S3. XRD patterns of Fe MOF and Ni-doped Fe MOF.

The crystal size was calculated for the FeF_2 and Ni doped FeF_2 catalysts were evaluated using the full width at half maximum (FWHM) and the angular position (2θmax) of the FeF_2 (110) peak according to the following Debye Scherrer equation:

$$L = \frac{k\lambda_{K\alpha 1}}{\beta_{(2\theta)} cos\theta_{max}} \qquad \beta = FWHM * \frac{\pi}{180} \qquad \theta = Theta * \frac{\pi}{180}$$

FeF_2:

$$L = \frac{\lambda_{K\alpha 1}}{\beta_{(2\theta)} cos\theta_{max}} = \frac{0.89 \times 0.15405}{0.437 \times \frac{\pi}{180} \times cos(13.386 \times \frac{\pi}{180})} = 17.98\ nm$$

Ni doped FeF_2:

$$L = \frac{\lambda_{K\alpha 1}}{\beta_{(2\theta)} cos\theta_{max}} = \frac{0.89 \times 0.15405}{0.593 \times \frac{\pi}{180} \times cos(13.455 \times \frac{\pi}{180})} = 13.25\ nm$$

Where L denotes the average particle size, $\lambda_{K\alpha 1}$ is the wavelength of X-ray radiation (0.15405 nm), θmax is the angular position at the FeF_2 (110) peak maximum, and $\beta_{(2\theta)}$ is the full width at half maximum (FWHM) of the peak broadening in radians.

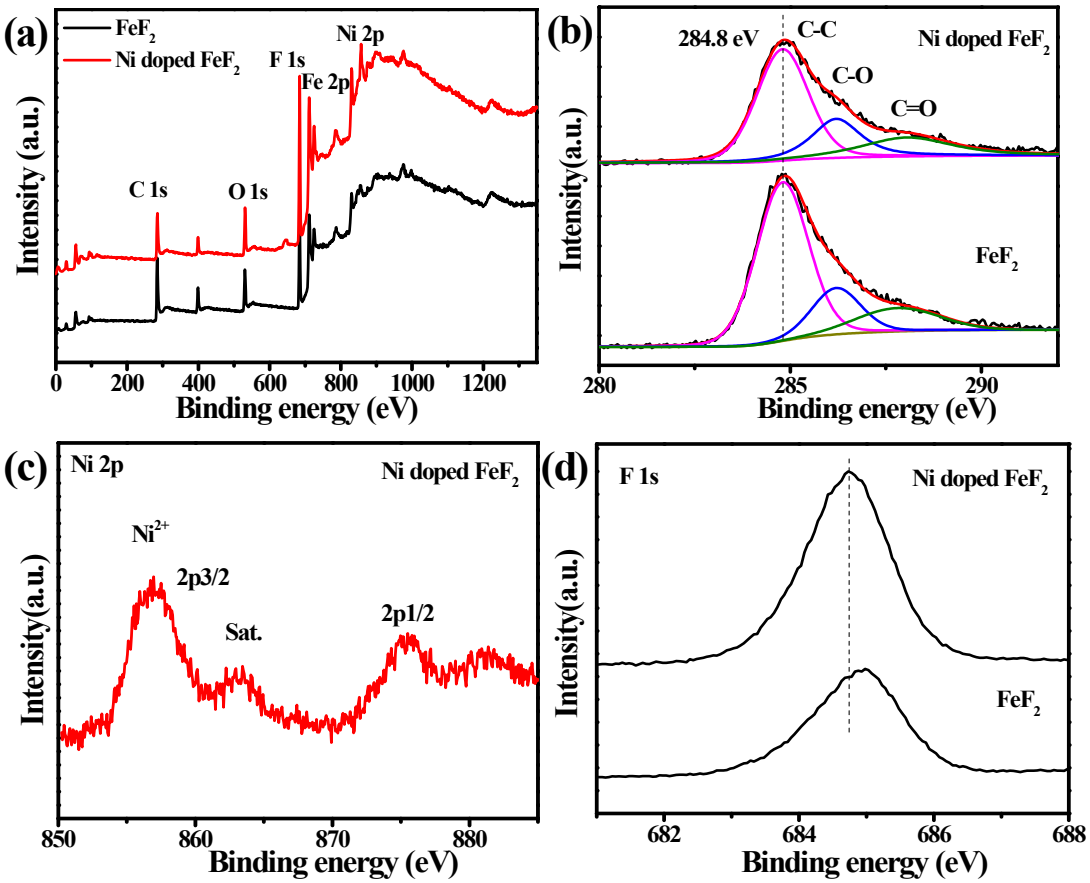

Figure S4. XPS survey spectrum (a) and High-resolution XPS spectra of C 1s (b) for FeF_2 and Ni-doped FeF_2, Ni 2p (c) for Ni doped FeF_2 and F 1s (d) for FeF_2 and Ni-doped FeF_2.

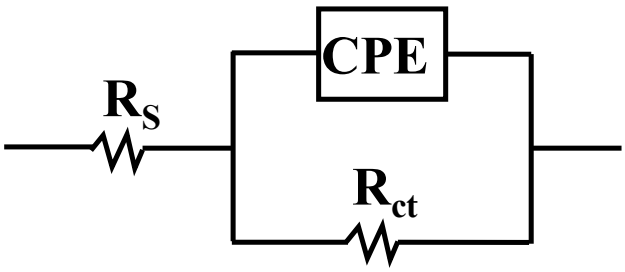

Figure S5a. Equivalent circuit diagram for fitting the EIS data.

R_s means uncompensated solution resistance, R_{ct} is a charge transfer resistance, and the CPE generally was employed to well fit the impedance data by safely treating as an empirical constant without considering its physical basis. And mostly, it was regarded as the double layer capacitor from the catalyst and catalyst solution.

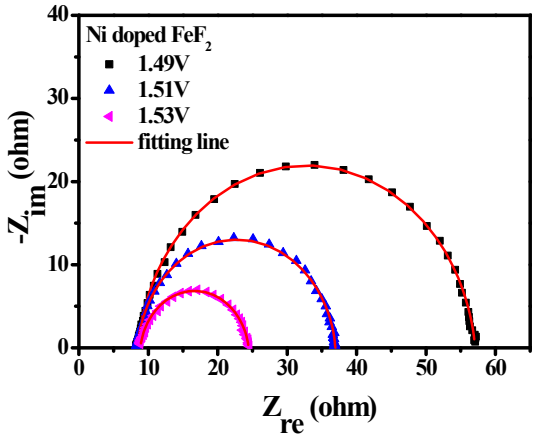

Figure S5b. Nyquist plots of EIS for Ni doped FeF_2 electrode obtained at three different potentials.

The fitting results were shown below.

EIS fitting parameters form equivalent circuits for Ni doped FeF_2 at three different potential in 1M KOH.

Potential/V	R_s/Ω	CPE/S s^{-n}	CPE-n	R_{ct}/Ω
1.49	8.50	1.077E-4	0.94	49
1.51	8.45	1.081E-4	0.94	28
1.53	8.85	1.256E-4	0.92	16

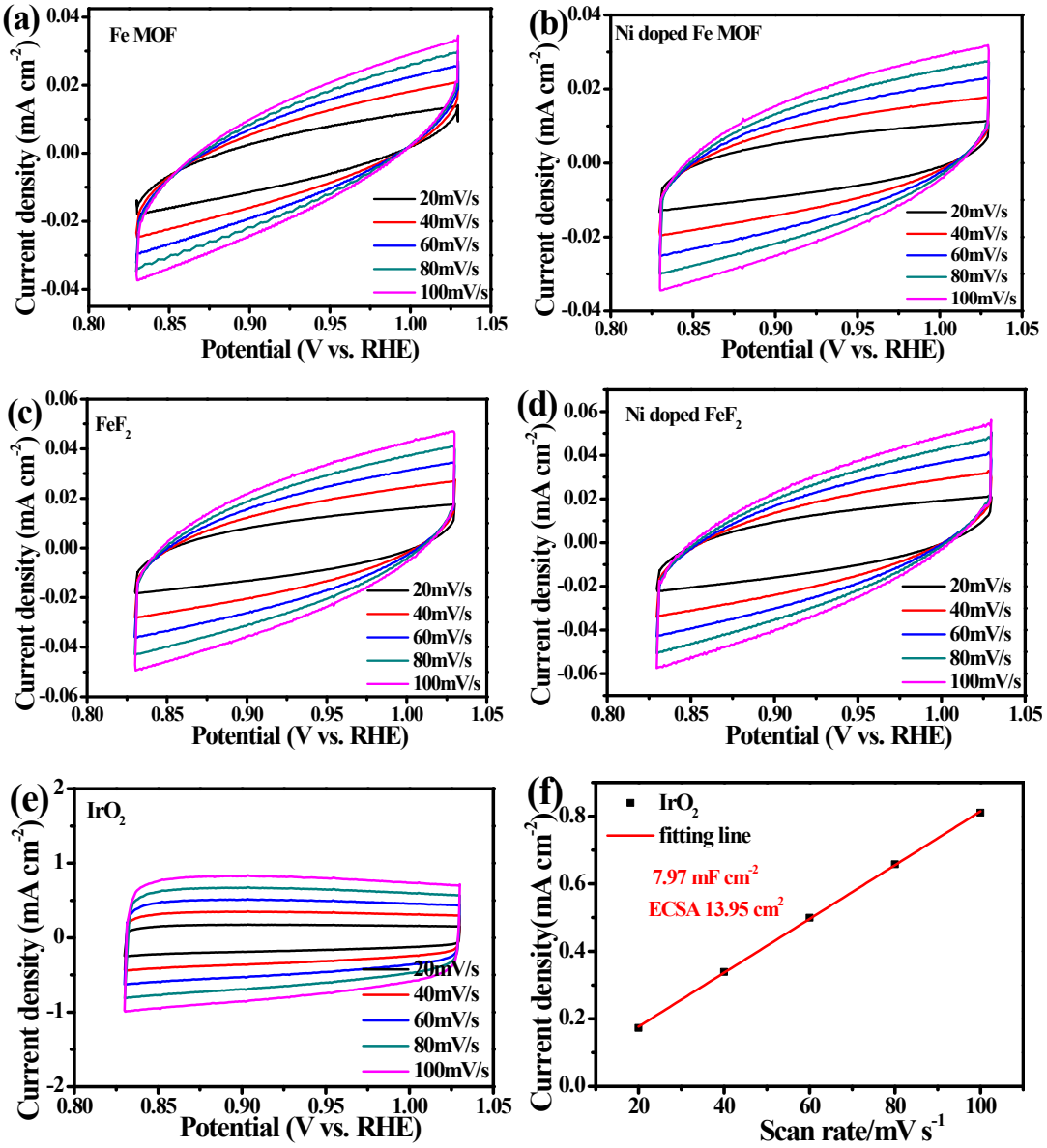

Figure S6. Cyclic voltammetry (CV) curves of Fe-MOF (a), Ni-doped MOF (b), FeF_2 (c), Ni-doped FeF_2 (d) and IrO_2 (e) with various scan rates (20–100 mV/s) in the 0.83 to 1.03V vs RHE region. Scan-rate dependence of the current densities derived from double-layer capacitance measurements of IrO_2 (f).

The electrochemical active surface area (ECSA) of IrO_2 was calculated to be 13.95 cm^2 for IrO_2 that was close to the reference reported.[7]

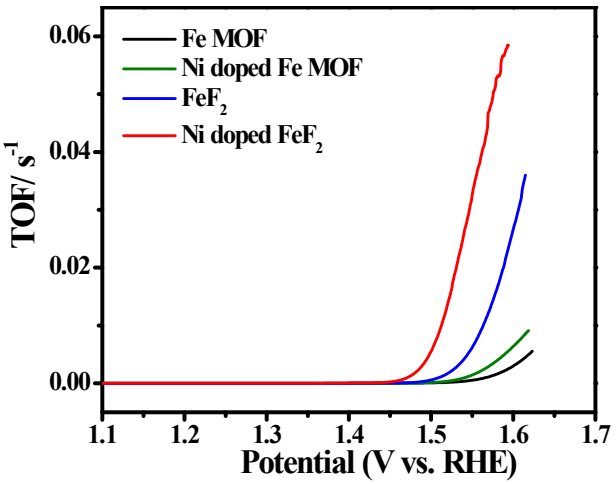

Figure S7. The turnover frequency curve for Fe MOF, Ni-doped Fe MOF, FeF_2 and Ni-doped FeF_2.

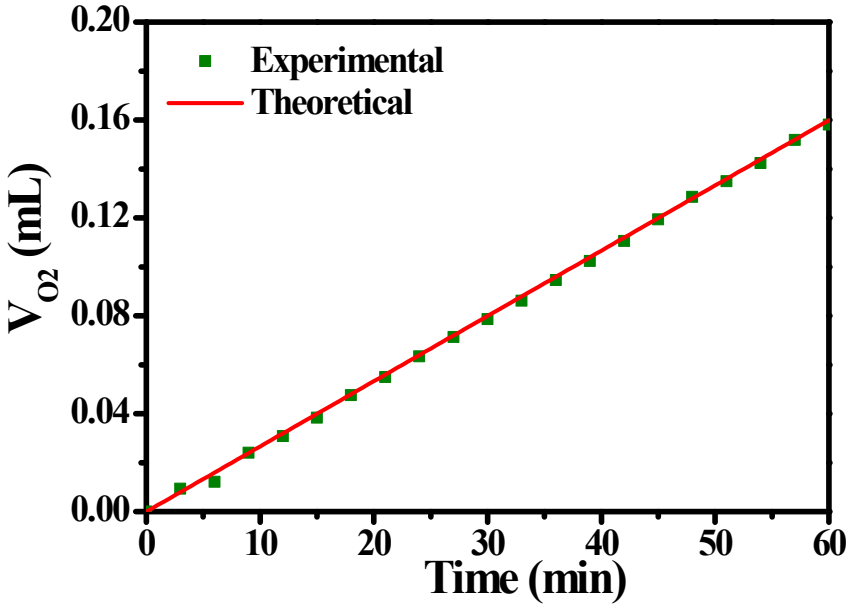

Figure S8. Faradic efficiency of oxygen evolution reaction activity for Ni doped FeF_2.

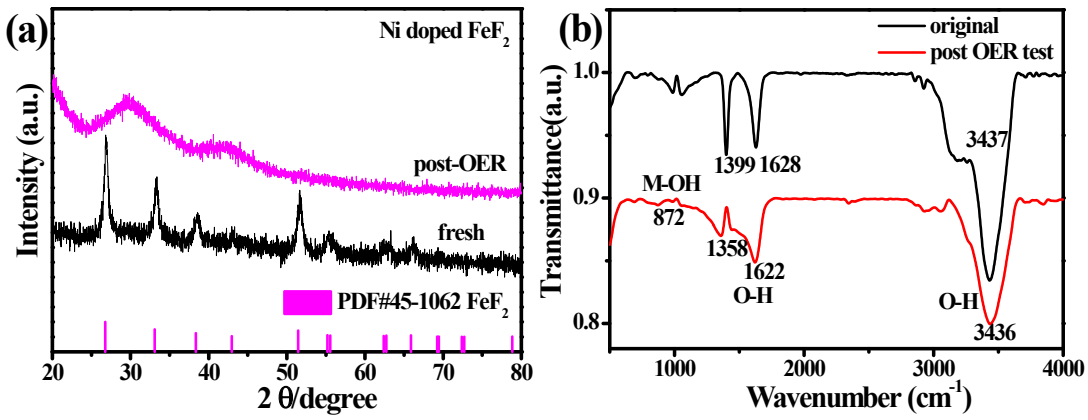

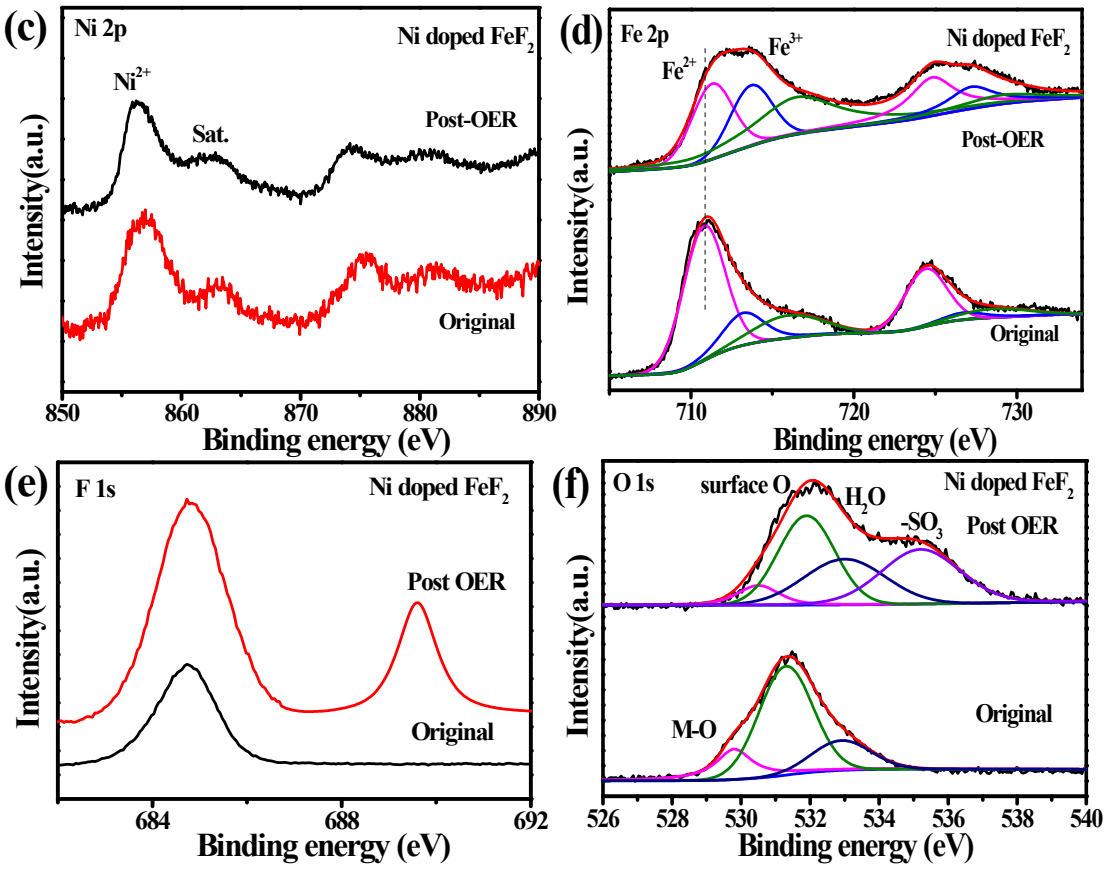

Figure S9. XRD patterns (a), Fourier transform infrared (FT-IR) spectra (b) and high-resolution XPS spectra in the Ni 2p (c), Fe 2p (d), F 1s (e) and O 1s region (f) for Ni-doped FeF_2 before and post OER test.

The infrared spectrum of Ni-doped FeF_2 before and after the OER test all showed three same main peaks. The band at 1399 cm^{-1} was from the carboxyl group. The O–H stretching vibration peaks (≈3440 cm^{-1}) and scissoring vibration peaks (1700–1500 cm^{-1}) were from water. A new band at about 872 cm^{-1} can be assigned to M–OH mode which appeared after OER test.[8-10]

Table S1. Elemental composition of FeF_2 and Ni-doped FeF_2 based on XPS.

Catalysts	Atomic composition (%)				
	Fe	Ni	F	O	C
FeF_2	9.01	/	21.9	14.57	54.52
Ni doped FeF_2	13.27	4.1	32.43	13.5	36.7

Due to the carbon contamination and the effect of conductive carbon tape used as substrate, the content of carbon was not accurate revealed by XPS. A misconception was done if the content of C is lower for the Ni doped FeF_2 than that of FeF_2. Actually, from the compositing analysis, the atomic ratio of Fe/F was around 0.41, indicating the stable composition of FeF_2.

Table S2. The binding energy of Fe 2p components for all samples.

Catalysts	Assignment	Binding energy/ eV	Relative intensity/ %
FeF_2	Fe(2+)	711.2	79.4
		724.8	
	Fe(3+)	713.6	20.6
		727.1	
Ni doped FeF_2	Fe(2+)	710.8	78.5
		724.4	
	Fe(3+)	713.2	21.5
		726.7	

Table S3. Comparison of OER performance of Ni doped FeF_2 with some Fe-based catalysts.

Catalysts	electrolytes	Overpetential (mV)/mA cm^{-2} for OER	references
Ni-doped FeF_2	1M KOH	275/η_{10}	This work
FeOOH@$Ni(OH)_2$	1M KOH	310/η_{10}	[11]
NiFe@NC	0.1M KOH	360/η_{10}	[12]
$Ni_{0.5}Fe_{0.5}$-HP	1M KOH	280/η_{10}	[13]
Co–Fe–P–Se/NC	1M KOH	270/η_{10}	[14]
Fe_3C@NCNT/NPC	1M KOH	340/η_{10}	[15]
$FeCo_3$ MOF-550	0.1 M KOH	390/η_{10}	[16]
N-doped FeP	1M KOH	440/η_{100}	[17]
FeCo-P/C	1M KOH	362/η_{10}	[18]
Fe–Co_3O_4/CNTs	1M KOH	300/η_{10}	[19]
FeS_x/CF	1M KOH	340/η_{10}	[20]
FeN_x/carbon	0.1 M KOH	360/η_{10}	[21]
Fe-doped NiO_x	1M KOH	310/η_{10}	[22]
NiCoFe-LDH/CFC	1M KOH	280/η_{10}	[23]
FeNi-P/GA	1M KOH	280/η_{10}	[24]
NiO/$NiFe_2O_4$	1 M KOH	302/η_{10}	[25]
NiFe-LDH	1 M KOH	290/η_{10}	[26]
Co^{II}Fe-ONC	1 M KOH	290/η_{50}	[27]
Ni/Fe_3O_4@ONC	1 M KOH	296 /η_{10}	[28]
α-Fe_2O_3@g-C_3N_4-NCs	0.5 M KOH	425/η_{10}	[29]
Ni_2Fe-O	1M KOH	370/η_{10}	[30]
Fe-Ni@NC-CNTs	1M KOH	274/η_{10}	[31]

NiFe-NC	1M KOH	271/η_{10}	[32]
Ni-Fe-P	1M KOH	271/η_{10}	[33]
$Ni_{0.75}Fe_{0.25}$ BDC	0.1 M KOH	310/η_{10}	[34]
Ni-Fe-O-S	1M KOH	272/η_{10}	[35]
$NiFe_x/NiFe_2O_4$@NC	1M KOH	262/η_{10}	[36]

Table S4. EIS fitting parameters form equivalent circuits for all samples at 1.51V in 1M KOH.

Catalysts	R_s/Ω	CPE/S s^{-n}	CPE-n	R_{ct}/Ω
Fe MOF	8.33	1.547E-5	0.89	412
Ni doped Fe MOF	9.58	3.335E-5	0.94	215
FeF_2	9.03	4.763E-5	0.93	75
Ni doped FeF_2	8.45	1.081E-4	0.94	28

Table S5. The binding energy of Fe 2p components for Ni-doped FeF_2 before and after the OER test.

Ni doped FeF_2	Assignment	Binding energy/ eV	Relative intensity/ %
Post OER	Fe(2+)	711.3	56.4
		724.9	
	Fe(3+)	713.7	43.6
		727.2	
Ni doped FeF_2	Fe(2+)	710.8	78.5
		724.4	
	Fe(3+)	713.2	21.5
		726.7	

References

1. K. Rui, G. Zhao, Y. Chen, Y. Lin, Q. Zhou, J. Chen, J. Zhu, W. Sun, W. Huang and S. X. Dou, *Adv. Funct. Mater.*, 2018, **28**, 1801554.
2. F. Zheng, D. Xiang, P. Li, Z. Zhang, C. Du, Z. Zhuang, X. Li and W. Chen, *ACS Sustainable Chem. Eng.*, 2019, **7**, 9743-9749.
3. J. Zhang, Z. Li, Y. Chen, S. Gao and X. W. Lou, *Angew. Chem., Int. Ed.*, 2018, **57**, 10944-10948.
4. C. C. L. McCrory, S. Jung, J. C. Peters and T. F. Jaramillo, *J. Am. Chem. Soc.*, 2013, **135**, 16977-16987.
5. M. Gao, W. Sheng, Z. Zhuang, Q. Fang, S. Gu, J. Jiang and Y. Yan, *J. Am. Chem. Soc.*, 2014, **136**, 7077-7084.
6. V. Balasubramani, S. Chandraleka, T. S. Rao, R. Sasikumar, M. R. Kuppusamy and T. M. Sridhar, *J. Electrochem. Soc.*, 2020, **167**, 037572.
7. G. Li, L. Anderson, Y. Chen, M. Pan and P.-Y. Abel Chuang, *Sustainable Energy & Fuels*, 2018, **2**, 237-251.
8. J. Qi, W. Zhang, R. Xiang, K. Liu, H.-Y. Wang, M. Chen, Y. Han and R. Cao, *Adv. Sci.*, 2015, **2**, 1500199.
9. L. Huang, X. Ge and S. Dong, *RSC Adv.*, 2017, **7**, 32819-32825.
10. K.-Y. Andrew Lin, H.-A. Chang and C.-J. Hsu, *RSC Adv.*, 2015, **5**, 32520-32530.
11. J. Wang, S. Li, R. Lin, G. Tu, J. Wang and Z. Li, *Electrochim. Acta*, 2019, **301**, 258-266.
12. L. Du, L. Luo, Z. Feng, M. Engelhard, X. Xie, B. Han, J. Sun, J. Zhang, G. Yin, C. Wang, Y. Wang and Y. Shao, *Nano Energy*, 2017, **39**, 245-252.
13. H. Qiao, Y. Yang, X. Dai, H. Zhao, J. Yong, L. Yu, X. Luan, M. Cui, X. Zhang and X. Huang, *Electrochim. Acta*, 2019, **318**, 430-439.
14. H. Wu, J. Wang, J. Yan, Z. Wu and W. Jin, *Nanoscale*, 2019, **11**, 20144-20150.
15. P. Zhao, X. Hua, W. Xu, W. Luo, S. Chen and G. Cheng, *Catal. Sci. Technol.*, 2016, **6**, 6365-6371.
16. Y. Han, J. Zhai, L. Zhang and S. Dong, *Nanoscale*, 2016, **8**, 1033-1039.
17. M. Yang, J.-Y. Xie, Z.-Y. Lin, B. Dong, Y. Chen, X. Ma, M.-L. Wen, Y.-N. Zhou, L. Wang

and Y.-M. Chai, *Appl. Surf. Sci.*, 2020, **507**, 145096.

18. W. Hong, M. Kitta and Q. Xu, *Small Methods*, 2018, **2**, 1800214.
19. H. Begum and S. Jeon, *Int. J. Hydrogen Energy*, 2018, **43**, 5522-5529.
20. W. Wang, R. Xu, B. Yu, X. Wang and S. Feng, *RSC Adv.*, 2019, **9**, 31979-31987.
21. J. Ding, P. Wang, S. Ji, H. Wang, V. Linkov and R. Wang, *Electrochim. Acta*, 2019, **296**, 653-661.
22. G. Wu, W. Chen, X. Zheng, D. He, Y. Luo, X. Wang, J. Yang, Y. Wu, W. Yan, Z. Zhuang, X. Hong and Y. Li, *Nano Energy*, 2017, **38**, 167-174.
23. T. Wang, W. Xu and H. Wang, *Electrochim. Acta*, 2017, **257**, 118-127.
24. A. V. Narendra Kumar, Y. Li, H. Yu, S. Yin, H. Xue, Y. Xu, X. Li, H. Wang and L. Wang, *Electrochim. Acta*, 2018, **292**, 107-114.
25. G. Liu, X. Gao, K. Wang, D. He and J. Li, *Int. J. Hydrogen Energy*, 2016, **41**, 17976-17986.
26. H. Zhong, T. Liu, S. Zhang, D. Li, P. Tang, N. Alonso-Vante and Y. Feng, *J. Energy Chem.*, 2019, **33**, 130-137.
27. P. Guo, Z. Wang, T. Zhang, C. Chen, Y. Chen, H. Liu, M. Hua, S. Wei and X. Lu, *Appl. Catal. B-Environ*, 2019, **258**, 117968.
28. G. Liu, R. Yao, Y. Zhao, M. Wang, N. Li, Y. Li, X. Bo, J. Li and C. Zhao, *Nanoscale*, 2018, **10**, 3997-4003.
29. O. Alduhaish, M. Ubaidullah, A. M. Al-Enizi, N. Alhokbany, S. M. Alshehri and J. Ahmed, *Sci. Rep.*, 2019, **9**, 14139.
30. Z. Xie, C. Zhang, X. He, Y. Liang, D. Meng, J. Wang, P. Liang and Z. Zhang, *Front. Chem.*, 2019, **7**.
31. X. Zhao, P. Pachfule, S. Li, J. R. J. Simke, J. Schmidt and A. Thomas, *Angew. Chem., Int. Ed.*, 2018, **57**, 8921-8926.
32. A. Kumar and S. Bhattacharyya, *ACS Appl. Mater. Interfaces*, 2017, **9**, 41906-41915.
33. C. Xuan, J. Wang, W. Xia, Z. Peng, Z. Wu, W. Lei, K. Xia, H. L. Xin and D. Wang, *ACS Appl. Mater. Interfaces*, 2017, **9**, 26134-26142.
34. Y. Hao, Q. Liu, Y. Zhou, Z. Yuan, Y. Fan, Z. Ke, C.-Y. Su and G. Li, *Energy Environ. Mater.*, 2019, **2**, 18-21.

35. C. Xuan, J. Wang, W. Xia, J. Zhu, Z. Peng, K. Xia, W. Xiao, Huolin L. Xin and D. Wang, *J. Mater. Chem. A*, 2018, **6**, 7062-7069.

36. J. Zhao, X. Zhang, M. Liu, Y.-Z. Jiang, M. Wang, Z.-Y. Li and Z. Zhou, *J. Mater. Chem. A*, 2019, **7**, 21338-21348.